Improving common bacterial blight phenotyping by using rub-inoculation and machine learning: cheaper, better, faster, stronger

Justine Foucher, Mylène Ruh, Martial Briand, Anne Préveaux, Florian Barbazange, Tristan Boureau, Marie-Agnès Jacques, Nicolas Chen

Improving common bacterial blight phenotyping by using rub-inoculation and machine learning: cheaper, better, faster, stronger

Justine Foucher[1], Mylène Ruh[1], Martial Briand[1], Anne Préveaux[1], Florian Barbazange[1], Tristan Boureau[1], Marie-Agnès Jacques[1] and Nicolas W. G. Chen[1]*.

[1]Univ Angers, Institut Agro, INRAE, IRHS, SFR QUASAV, F-49000 Angers, France.

* Correspondence to: nicolas.chen@agrocampus-ouest.fr

Keywords: phenotyping, plant disease, bacterial blight, *Xanthomonas,* TAL effectors, *Phaseolus vulgaris*.

ABSTRACT

Accurate assessment of plant symptoms plays a key role for measuring the impact of pathogens during plant-pathogen interaction. Common bacterial blight caused by *Xanthomonas phaseoli* pv. *phaseoli* and *Xanthomonas citri* pv. *fuscans* (*Xpp-Xcf*) is a major threat to common bean. The pathogenicity of these bacteria is variable among strains, and depends mainly on a type III secretion system and associated type III effectors such as transcription activator-like effectors (TALEs). Because the impact of a single gene is often small and difficult to detect, a discriminating methodology is required to distinguish the slight phenotype changes induced during the progression of the disease. Here, we compared two different inoculation and symptom assessment methods for their ability to distinguish two *tal* mutants from their corresponding wild-type strains. Interestingly, rub-inoculation of the first leaves combined with symptom assessment by machine learning-based imaging allowed significant distinction between wild-type and mutant strains. By contrast, dip-inoculation of first trifoliate leaves combined with chlorophyll fluorescence imaging did not differentiate the strains. Furthermore, the new method developed here led to the miniaturization of pathogenicity tests and significant time savings.

INTRODUCTION

Monitoring the impact of pathogens on plants is essential for improving knowledge on plant-pathogen interactions and developing effective management practices (Bock et al., 2010). Assessing plant symptoms is a key step in detecting plant resistance or evaluating the virulence of a pathogen. Pathogenicity tests must give homogeneous and reproducible results and use an objective method of symptom assessment to be interpretable (Nutter et al., 2006). Visual symptom assessment is a simple and easily accessible method used in many studies of plant-pathogens interactions. However, it lacks objectivity, accuracy and precision (Bock et al., 2008; Poland and

Nelson, 2010). The recent development of different optical techniques has allowed to automate the process of symptom assessment while ensuring a standardization of results (Mahlein, 2016). As such, computational image analysis provides a more objective, accurate, reproducible and quantitative measure of disease severity than visual assessment.

Common bacterial blight of bean (CBB) is a significant bacterial disease on common bean, with yield losses of more than 40% under favorable conditions (Belete and Bastas, 2017; Rodríguez De Luque and Creamer, 2014). Symptoms can occur on leaves, stems, pods and seeds (Zaumeyer and Thomas, 1957). Leaf symptoms initially appear as water-soaked spots, which enlarge and can coalesce with adjacent lesions (Goodwin and Sopher, 1994). Foliar lesions are often surrounded by a chlorotic halo and evolve in necrosis, possibly resulting in the death of the entire leaf and partial defoliation of the plant. Water-soaked spots and necrosis can also be observed on pods and seeds. These symptoms evolve in dark red-brown lesions that are generally circular and slightly sunken (Vidaver, 1993).

To phenotype CBB symptoms, different organs (seeds, pods, first leaves, trifoliate leaves, stems) can be inoculated in different ways. In particular, leaves can be inoculated by dipping, spraying, rubbing, multiple needles or infiltration (Aggour et al., 1989; Popovic et al., 2012). Traditionally, symptoms of CBB were assessed by visual evaluation using different rating scales based on a visual estimation of the percentage of infected leaf area (Aggour et al., 1989; Cafati and Saettler, 1980; Opio et al., 1993; Pastor-Corrales et al., 1981; Zapata, 2006). In 2012, it was shown that assessment of CBB symptoms by RGB image analysis was more reproducible and more objective than a rating scale, and presented a high differentiation power between plant genotypes (Xie et al., 2012). Another method was developed based on leaf inoculation by dipping combined with chlorophyll fluorescence imaging (Rousseau et al., 2013). This assessment method was successfully used to

discriminate different degrees of resistance in common bean against *Xpp-Xcf* (Foucher et al., 2020; Rousseau et al., 2013).

CBB is caused by *Xanthomonas phaseoli* pv. *phaseoli* (*Xpp*) and *Xanthomonas citri* pv. *fuscans* (*Xcf*) (Chen et al., 2021; Constantin et al., 2016). Pathological convergence of these two pathovars is probably due to extensive horizontal gene transfers, which led to genomic regions sharing 100% nucleotide identity between *Xpp* and *Xcf* (Aritua et al., 2015; Chen et al., 2018). These homologies allowed the development of specific molecular tools for detecting both *Xpp* and *Xcf* on seed lots (Audy et al., 1994; de Paiva et al., 2020; Grimault et al., 2014). Different *Xpp-Xcf* strains may have different levels of pathogenicity regardless of whether they belong to one or the other pathovars (Mkandawire et al., 2004). In addition, common bean resistance to CBB is mediated by numerous quantitative trait loci (Monteiro et al., 2020; Singh and Miklas, 2015; Yu et al., 2012). Differences in aggressiveness combined with the presence of quantitative resistances lead to a wide range of possible disease intensities (Duncan et al., 2011). Thus, the interaction between common bean and *Xpp-Xcf* must be finely phenotyped, in order to detect these variations as accurately as possible.

The pathogenicity of *Xanthomonas* is partly mediated by a type III secretion system (T3SS) and associated type III effectors (T3Es) (An et al., 2019; Büttner and Bonas, 2010). Among T3Es, *Xanthomonas* bacteria possess transcription activator-like effectors (TALEs). TALEs are injected inside the plant cell via the T3SS and migrate to the nucleus where they are able to induce targeted genes of the plant, often leading to disease enhancement (Boch and Bonas, 2010). Nine different TALE-encoding genes and alleles were discovered in *Xpp-Xcf* (Ruh et al., 2017). *Xcf* strain 6165R possesses only one *tal* gene named *tal22B* while *Xpp* strain 6546R bears two *tal* genes named *tal19I* and *tal18H*.

In this study, we generated *tal* mutant strains 6165RΔ*tal22B* and 6546RΔ*tal18H*. Then, the pathogenicity of strains 6165R and 6546R were compared to each other and to their corresponding

tal mutants. For this, we used two different tests to phenotype CBB symptoms in controlled conditions. The first method corresponded to the method developed by Rousseau et al. (2013), consisting of dipping the first trifoliate leaf in bacterial suspension followed by chlorophyll fluorescence imaging (CFI). The second method corresponded to a new pathogenicity test consisting of rub-inoculation of the first leaves and evaluation of symptoms by machine learning-trained imaging (MLI). MLI was performed on RGB images using the ilastik software (Berg et al., 2019), which was recently exploited in biomedical and environmental studies as well as plant symptoms assessment (Ilett et al., 2020; Ojeda-Martinez et al., 2020; Pike et al., 2020; Rashid et al., 2019).

MATERIALS AND METHODS

Bacterial strains and growth conditions

Xanthomonas phaseoli pv. *phaseoli* strain 6546R and *Xanthomonas citri* pv. *fuscans* strain 6165R are rifamycin-resistant derivatives of strains CFBP6546 and CFBP6165 respectively. Strains were grown at 28 °C for 48 h on trypticase soy agar (TSA) medium (17.0 $g.L^{-1}$ pancreatic digest of casein; 3.0 $g.L^{-1}$ enzymatic digest of soy bean; 5.0 $g.L^{-1}$ NaCl; 2.5 $g.L^{-1}$ K_2HPO_4; 2.5 $g.L^{-1}$ glucose; 15 $g.L^{-1}$ agar), then at 28 °C for 24 h on TSA10 (a 1/10 dilution of TSA, except for agar maintained at 15 $g.L^{-1}$) to obtain fresh bacterial cultures. Media were supplemented by rifamycin (50 mg. L^{-1}) for selection.

Mutagenesis of *tal* genes and validation of mutants

Plasmid pK18mob::sacB (Schäfer et al., 1994) was used to generate marker-free deletion mutants of *tal22B* in strain 6165R or *tal18H* in strain 6546R. First, specific primers (Table S1) were designed according to whole genome data (Ruh et al., 2017), to amplify the flanking regions of

each *tal* gene by PCR using the PHusion® High Fidelity DNA polymerase (Finnzymes,Waltham, MA, USA) following the manufacturer's instructions. For each *tal* gene, PCR products were purified using the Wizard® SV Gel and PCR Clean-Up System (Promega), then cloned in tandem into the suicide plasmid pK18mob::sacB using digestion by *Bsa*I enzyme and ligation by T4 DNA ligase. Recombinant plasmids were electrostransferred into competent 6165R or 6546R strains. Primary transformants were immediately grown in liquid MOKA medium (yeast extract 4 $g.L^{-1}$; casamino acids 8 $g.L^{-1}$; KH_2PO_4 2 $g.L^{-1}$; $MgSO_4.7H_2O$ 0.3 $g.L^{-1}$) for two hours at 28°C without selection, then plated on MOKA agar medium supplemented with kanamycin (50 $\mu g.mL^{-1}$). Kan^r colonies were then plated on MOKA medium supplemented with kanamycin and sucrose at 10% for selecting secondary recombinants. Resulting colonies were tested for deletion of *tal* genes by DNA extraction followed by PCR and sequencing.

Two additional analyses were done to validate *tal* mutants. First, to confirm that TALE proteins corresponding to deleted genes were not produced, Western Blot assays were performed. Briefly, total proteins were extracted from 0.4 mL of overnight bacterial suspensions and migrated by Sodium Dodecyl Sulfate – Polyacrylamid Gel Electrophoresis (SDS-PAGE), then immunoblotted with a primary anti-TALE antibody. The anti-TALE antibody was raised in rabbit against an *E. coli*-produced designer TALE protein composed of the N-terminal domain of a TALE protein plus six repeats (I. Fuentes and L. Noël, unpublished). TALE backbone was derived from the *hax3* tal gene sequence from X. campestris pv. campestris strain Xca5 as described (Streubel et al., 2012). Second, to check the influence of deletion on the growth capacity of the mutants, bacterial growth control was performed. For this, liquid cultures at initial concentration of 1×10^6 $CFU.mL^{-1}$ were prepared in TS10 broth, and the absorbance (λ = 600nm) was monitored every 8 or 30 min using a Labsystem Bioscreen C system, over an incubation period of 35 h at 28°C under shaking at 200 rpm. Each strain was controlled with technical triplicates and biological duplicates.

130

131 **Genome sequencing, assembly and annotation**

132 Genomic DNA of strains 6546RΔ*tal18H* and 6165RΔ*tal22B* was extracted with the Wizard®
133 Genomic DNA Purification Kit (Promega, Madison, USA) according to the manufacturer's
134 recommendations. PacBio Single Molecule Real Time (SMRT) sequencing was performed at the
135 Icahn School of Medicine at Mount Sinai (New York, USA) using one SMRT cell per strain to
136 achieve ~100× coverage. De novo assembling was performed using the following procedure. Reads
137 were filtered using PreAssembler Filter v1 of the SMRT Portal version 2.3 (Pacific Biosciences of
138 California, Inc.), with Minimum Subread Length 500, Minimum Polymerase Read Quality 0.80
139 and Minimum Polymerase Read Length 100. Assembly was performed using Canu v1.5 (Koren et
140 al., 2017). Circularisation was done using Berokka v0.2.3 (https://github.com/tseemann/berokka).
141 Sequence start was fixed using the Fixstart command of Circlator v1.5.1 (Hunt et al., 2015).
142 Polishing was performed using the variantCaller tool
143 (https://github.com/PacificBiosciences/GenomicConsensus) with --algorithm best. Whole genome
144 sequences of wild-type strains 6165R and 6546R (Briand et al., submitted) were used for
145 comparative analyses. Annotation of whole genome assemblies was performed with Prokka
146 v1.14.6 (Seemann, 2014). Average nucleotide identity analyses between genomes of wild-type and
147 TALE-deleted strains were performed with pyANI (Pritchard et al., 2016).

148

149 **Plant materials and growing conditions**

150 Seeds of the susceptible common bean cultivar JaloEEP558 were obtained from the Center for
151 Tropical Agriculture (CIAT, Colombia), available under accession number G9603
152 (http://genebank.ciat.cgiar.org/genebank/main.do). Plants were sown in plastic pots (7 × 7 × 8 cm)
153 containing pre-wetted soil. The sowings were covered with a P17 veil for four days for

154 homogenized germination. Plants were grown in a growth chamber at 23°C/20°C (day/night) with
155 a relative humidity of 80% and a photoperiod of 16 hours. Plants were watered every two days with
156 water for the first seven days, then with a nutrient solution (7.5-5-15 N-P-K) for up to 15 days, and
157 with a richer nutrient solution (15-10-30 N-P-K) until the end of the trial. The day before
158 inoculation, relative humidity and temperature were increased at 95% and 28°C/25°C (day/night)
159 to provide adequate conditions for infection. On the third day after inoculation, humidity was
160 reduced to 80% until the end of the assay.
161
162 **Pathogenicity assays**
163 For both methods, bacterial suspensions were calibrated at 1×10^7 CFU.mL^{-1} in sterile distilled
164 water, and symptoms were monitored two weeks after inoculation. Each pathogenicity test was
165 performed twice independently.
166 For phenotyping by chlorophyll fluorescence imaging (CFI), inoculations were performed at stage
167 V1 (first trifoliolate leaf unfolded) by dipping the first trifoliate leaf for 30 s into bacterial
168 suspensions or water as control. Symptom development was monitored by CFI at the PHENOTIC
169 Seeds and Plants platform of the IRHS in Angers (France) as described in Rousseau et al. (2013).
170 Briefly, inoculated leaflets were collected and set in the dark for 30 min. Then, for each leaflet, a
171 first picture was taken under a modulated flash of light to measure basal fluorescence (F0) of the
172 tissues, followed by another picture taken under a high flash of saturating light to measure the
173 maximum fluorescence emission level (Fm). For each pixel, the maximum quantum yield of
174 photosystem II photochemistry (Fv/Fm = (Fm-F0)/Fm) was calculated using Phenoplant
175 (http://www.phenoplant.org) to discriminate diseased and healthy leaflet areas (Rousseau et al.,
176 2015). For each plant, results correspond to the mean disease area percentage of the three leaflets
177 coming from the same inoculated leaf.

For phenotyping by machine learning-trained imaging (MLI), inoculations were performed by rub-inoculation on the two first leaves of eight-day-old plants. Rub-inoculation consisted of one passage of a gloved finger dipped in bacterial suspension or water as control. For each leaf, two inoculations were done on the limb on each side of the central vein. To evaluate the symptoms, detached leaves were put on a LED light table of 1,600 lumen and images were taken with a fixed-height digital camera (Canon EOS 700D, Canon Inc., Taiwan) and saved as JPEG files. Each image comprised the two first leaves of a same plant, each rubbed twice, thus representing four technical replicates. Machine learning-based pixel segmentation was performed using the Pixel Classification workflow from ilastik v1.3.3 (Berg et al., 2019). Training was performed using 14 features including color/intensity, edge and texture, on 37 images representative of the whole dataset in terms of leaf colour and intensity of symptoms (training file available upon request). Three labels were used for discriminating the background, leaf tissues and symptoms. Symptoms corresponded to both chlorosis and necrotic tissues, as assessed by expert eye analysis. After the training, batch processing of all images was performed. Pixel quantification was done using FiJi (Schindelin et al., 2012). Briefly, labels were retrieved using the "Image threshold" option. Then, the "Analyse particle" command was used to quantify pixels corresponding to either the background or the symptoms. Total leaf areas were retrieved by subtracting background pixels from the total image pixels.

RESULTS

Phenotyping of strains with different degrees of pathogenicity

For both inoculation methods, more severe symptoms appeared after inoculation of strain 6546R than strain 6165R (Fig. 1). However, statistical distinction between strains was superior using rub-inoculation with MLI ($p < 0.01$) than dip-inoculation with CFI ($p > 0.05$). The differences observed

between both methods could be explained by the inoculation method itself, which appeared as playing a major role in the homogeneity of the symptoms. Indeed, dip inoculation of trifoliates led to symptoms developing mainly from the margins, being unevenly distributed over the leaflets and evolving into more or less extended patches hardly distinguishable between leaves inoculated by one strain or the other (Fig. 1b and c). Moreover, the occurrence of symptoms was stochastic as symptoms did not appear evenly on all leaflets of the same leaf, meaning that the variability between leaflets was even higher than between individuals in some cases (not shown). In contrast, symptoms were clearly distinguishable between both strains after rub inoculation (Fig. 1e and f). For strain 6165R, symptoms appeared as tiny spots evenly distributed across the whole inoculated area, likely caused by bacteria entering through openings corresponding to trichomes damaged by the rubbing. For strain 6546R, most of the spots coalesced, leading to large symptomatic areas. In all, rub-inoculation produced more homogeneous and reproducible symptoms than dip-inoculation. To test if CFI could be used for assessing symptoms on rub-inoculated leaves, we compared CFI and MLI after rub-inoculation of first leaves with strain 6165R (Supp. Fig. 1). While chlorotic areas were accurately retrieved with both image acquisition methods, CFI failed to detect the tiny spots corresponding to early symptoms. Moreover, CFI tended to take into account pixels outside the inoculated area, thus not corresponding to symptoms caused by the bacteria (e.g. the petiole), which was not the case for MLI. Therefore, MLI was more suited than CFI to detect symptoms on rub-inoculated plants.

Description of *tal* mutants

To further evaluate the discriminating power of each symptom assessment method, we constructed two deletion mutants of *tal* genes named 6546RΔ*tal18H* and 6165RΔ*tal22B*. Both 6546RΔ*tal18H* and 6165RΔ*tal22B* were unable to produce TAL18H or TAL22B proteins, respectively (Fig. 2a

and b). PacBio SMRT sequencing allowed us to compare the complete genome sequences of the mutants to their corresponding wild-type strains. In both cases, an average nucleotide identity of more than 99.99% was found between the wild-type strains and their mutants, indicating that no major modification occurred in the mutant strains.

As described before, both *tal22B* and *tal18H* are located on plasmids (Ruh et al., 2017). In strain 6165RΔ*tal22B*, the deletion of *tal22B* was restricted to a clean gap of 3,915 bp in plasmid A corresponding to *tal22B* from start to stop (Fig. 2d). In strain 6546R, plasmid C comprised a gap encompassing *tal18H* plus 2137 bp (Fig. 2c) including three genes encoding short (60 to 107 aminoacid-long) hypothetical proteins (not shown). For this strain, directed mutagenesis failed until we tested more than 350 clones for *tal18H* deletion. The deletion was flanked by identical *ISXac2* insertion sequences (IS) suggesting that it occurred through recombination between IS (Fig. 2c). Therefore, 6546RΔ*tal18H* corresponded to a variant of strain 6546R presenting a spontaneous deletion of *tal18H* on plasmid C. For both strains, the deletion had no major effect on the bacterial growth of the mutants compared to the wild-type strains in TS10 medium (Fig. 2e and f).

Virulence evaluation of wild-type and mutant strains

With both methods, the mutant strains led to less symptoms than the corresponding wild-type strains, suggesting that *tal18H* and *tal22B* were involved in the pathogenicity of strains 6546R and 6165R, respectively (Fig. 3 and 4). However, rub-inoculation with MLI significantly discriminated the two mutants from corresponding wild-type strains ($p < 0.05$), while dip-inoculation with CFI did not ($p > 0.1$). Interestingly, the accuracy of rub-inoculation followed by MLI was high enough to discriminate between strains presenting very low aggressiveness. Indeed, only 2% or 1% of the total leaf pixels corresponded to symptoms after inoculation with 6165R or 6165RΔ*tal22B*, respectively, which further demonstrated the discriminative power of this method.

250

251 **Phenotyping of symptoms after leaf dipping**

252 Although training was done on images of rub-inoculated primary leaves, we tested if MLI could
253 discriminate symptoms on trifoliate leaves after inoculation by dipping. For this, we performed
254 both CFI and MLI on images taken from the same dip-inoculated plants (one image per leaflet).
255 We compared the CFI and MLI results to expert symptom assessment by eye using the reference
256 scale of Opio *et al*. (1993). Globally, MLI was able to detect most of the CBB symptoms retrieved
257 by eye, while CFI detected comparatively less visible symptoms than the two other methods (Supp.
258 Fig. 2). In accordance with this, correlation of visual assessment with MLI was stronger than with
259 CFI (Fig. 5). The high linear correlation found between visual assessment and MLI ($R^2 > 0.96$)
260 demonstrates that the MLI training developed in this study is a good estimator for symptom
261 quantification on dip-inoculated leaves.

262

263 **DISCUSSION**

264 Our study highlights that rub-inoculation on first leaves combined with MLI represents a fast,
265 simple and efficient way to quantify the fine symptom differences existing between strains
266 differing by only one or few genes. The two *tal* mutants constructed here induced less symptoms
267 than the wild-type strains, suggesting that TAL18H and TAL22B participate in the pathogenicity
268 of strains 6546R and 6165R, respectively. However, cloning of *tal* genes and complementation of
269 these strains is needed to confirm the role of these TALEs, especially because genes other than *tal*
270 were missing in strain 6546RΔ*tal18H*.

271 In addition to the gain of discriminating power, the rub-inoculation method presented several other
272 advantageous characteristics compared to dip-inoculation. First, the time required to carry out a
273 trial was reduced (Table 1). Indeed, the use of first leaves instead of first trifoliates saved one week

of plant growing time, leading to a 22-day trial instead of a month. Moreover, the growth of first leaves was often more homogeneous than that of first trifoliate leaves. Consequently, for a same number of plants sown, more can be used for a pathogenicity test on first leaves than first trifoliates. This can be an important factor for trials under controlled greenhouse conditions, where the space available is often limited. In addition, the average inoculation time per plant (including all time spent in the growth chamber) was three times longer for dip-inoculation than rub-inoculation (Table 1), as it required more handling time and a 30-second immersion of the leaf in the bacterial suspension. Furthermore, the volume of inoculum required was 20 times less for rub-inoculation than dip-inoculation. Therefore, less material was needed for rub-inoculation and the waste was easier to process. Finally, MLI requires simple materials such as a digital camera, a tripod and a LED table, which can be afforded quite easily. On the other hand, CFI requires a complete fluorescence imaging system that is much more expensive to purchase and maintain. The shooting of plants (including handling time) was also more than three time longer for chlorophyll fluorescence than RGB picture taking. This was mainly due to CFI requiring the leaves to be kept in the dark for 30 minutes prior shooting, then perform the shootings leaflet by leaflet in a dark room, while RGB pictures were done with both first leaves together.

Although the method developed here presents many advantages for symptom quantification, it is important to note that chlorophyll fluorescence imaging is able to detect non-visible symptoms resulting from a disruption of photosynthesis during the early stages of infection and has a potential to discriminate between strains differing by a single gene (Méline et al., 2020). The future development of pipelines combining different phenotyping methods will undoubtedly contribute to analyze more in-depth the complex contributions of single or multiple genes to the virulence of plant pathogens.

ACKNOWLEDGMENTS

We warmly thank Céline Rousseau and Guillaume Lebreton from the PHENOTIC platform (IRHS, Beaucouzé, France) for their help in the analysis of chlorophyll fluorescence images, Daniel Sochard (IRHS, Beaucouzé, France) for technical help for *in planta* experiments, Armelle Darrasse (IRHS, Beaucouzé, France) for valuable advices during *tal* mutagenesis, and Ivanna Fuentes, and Laurent Noël (LIPME, Toulouse, France) for contributing an anti-TALE antibody. The authors also thank the French Network on Xanthomonads (FNX) (https://www.reseau-xantho.org/) for recurrent scientific exchanges and methods sharing.

This study was supported by the French National Research Agency CROpTAL project (ANR-14-CE19–0002-04). JF was funded by a PhD grant (BRUTAL project) from the French National Research Institute for Agriculture (INRAE) and the region Pays de la Loire, France. MR was funded by a PhD grant (X-HOT project) from Angers-Loire Metropole, France. The funding bodies did not participate in any of the study design, data collection and analysis, or writing the manuscript.

PacBio sequencing was performed at Icahn School of Medicine at Mount Sinai (NY, USA) under the supervision of Robert Sebra, and preliminary quality control of DNA was performed at the ANAN platform from the SFR 4207 QUASAV (Angers, France). Bacterial strain preservation and supply was ensured by the CIRM-CFBP (Beaucouzé, INRAE, France).

DATA AVAILABILITY STATEMENT

The data and materials that support the findings of this study (ilastik training file and bacterial strains) are available from the corresponding author upon request. The whole genome sequences of strains 6546RΔ*tal18H* and 6165RΔ*tal22B* were deposited to GenBank under accession numbers CP072393-CP072395 and CP072396-CP072397, respectively.

322

323 **REFERENCES**

324 Aggour, A. R., Coyne, D. P., and Vidaver, A. K. (1989). Comparison of leaf and pod disease
325 reactions of beans (Phaseolus vulgaris L.) inoculated by different methods with strains of
326 Xanthomonas campestris pv. Phaseoli (Smith) dye. *Euphytica* 43, 143–152.
327 doi:10.1007/BF00037907.
328 An, S. Q., Potnis, N., Dow, M., Vorhölter, F. J., He, Y. Q., Becker, A., et al. (2019). Mechanistic
329 insights into host adaptation, virulence and epidemiology of the phytopathogen
330 Xanthomonas. *FEMS Microbiol. Rev.* 44, 1–32. doi:10.1093/femsre/fuz024.
331 Aritua, V., Harrison, J., Sapp, M., Buruchara, R., Smith, J., and Studholme, D. J. (2015). Genome
332 sequencing reveals a new lineage associated with lablab bean and genetic exchange between
333 Xanthomonas axonopodis pv. phaseoli and Xanthomonas fuscans subsp. fuscans. *Front.*
334 *Microbiol.* 6, 1–18. doi:10.3389/fmicb.2015.01080.
335 Audy, P., Laroche, A., Saindon, G., Huang, H. C., and Gilbertson, R. L. (1994). Detection of the
336 bean common blight bacteria, Xanthomonas campestris pv. phaseoli and X.c.phaseoli var.
337 fuscans, using the polymerase chain reaction. *Phytopathology* 84, 1185–1192.
338 doi:10.1094/phyto-84-1185.
339 Belete, T., and Bastas, K. K. K. (2017). Common Bacterial Blight (Xanthomonas axonopodis pv.
340 phaseoli) of Beans with Special Focus on Ethiopian Condition. *J. Plant Pathol. Microbiol.*
341 08, 403. doi:10.4172/2157-7471.1000403.
342 Berg, S., Kutra, D., Kroeger, T., Straehle, C. N., Kausler, B. X., Haubold, C., et al. (2019).
343 Ilastik: Interactive Machine Learning for (Bio)Image Analysis. *Nat. Methods* 16, 1226–
344 1232. doi:10.1038/s41592-019-0582-9.
345 Boch, J., and Bonas, U. (2010). Xanthomonas AvrBs3 family-type III effectors: Discovery and

346 function. *Annu. Rev. Phytopathol.* 48, 419–436. doi:10.1146/annurev-phyto-080508-081936.
347 Bock, C. H., Parker, P. E., Cook, A. Z., and Gottwald, T. R. (2008). Visual rating and the use of
348 image analysis for assessing different symptoms of citrus canker on grapefruit leaves. *Plant*
349 *Dis.* 92, 530–541. doi:10.1094/PDIS-92-4-0530.
350 Bock, C. H., Poole, G. H., Parker, P. E., and Gottwald, T. R. (2010). Plant disease severity
351 estimated visually, by digital photography and image analysis, and by hyperspectral
352 imaging. *CRC. Crit. Rev. Plant Sci.* 29, 59–107. doi:10.1080/07352681003617285.
353 Büttner, D., and Bonas, U. (2010). Regulation and secretion of Xanthomonas virulence factors.
354 *FEMS Microbiol. Rev.* 34, 107–133. doi:10.1111/j.1574-6976.2009.00192.x.
355 Cafati, C. R., and Saettler, A. W. (1980). Effect of Host on Multiplication and Distribution of
356 Bean Common Blight Bacteria. *Phytopathology* 70, 675–679. doi:10.1094/phyto-70-675.
357 Chen, N. W. G., Ruh, M., Darrasse, A., Foucher, J., Briand, M., Costa, J., et al. (2021). Common
358 bacterial blight of bean: a model of seed transmission and pathological convergence. *Mol.*
359 *Plant Pathol.* in press.
360 Chen, N. W. G., Serres-giardi, L., Ruh, M., Briand, M., Bonneau, S., Darrasse, A., et al. (2018).
361 Horizontal gene transfer plays a major role in the pathological convergence of Xanthomonas
362 lineages on common bean. *BMC Genomics* 19, 606. Available at:
363 https://doi.org/10.1186/s12864-018-4975-4.
364 Constantin, E. C., Cleenwerck, I., Maes, M., Baeyen, S., Van Malderghem, C., De Vos, P., et al.
365 (2016). Genetic characterization of strains named as Xanthomonas axonopodis pv.
366 dieffenbachiae leads to a taxonomic revision of the X. axonopodis species complex. *Plant*
367 *Pathol.* 65, 792–806. doi:10.1111/ppa.12461.
368 de Paiva, B. A. R., Wendland, A., Teixeira, N. C., and Ferreira, M. A. S. V. (2020). Rapid
369 Detection of Xanthomonas citri pv. Fuscans and Xanthomonas phaseoli pv. Phaseoli in

Common Bean by Loop-Mediated Isothermal Amplification. *Plant Dis.* 104, 198–203. doi:10.1094/PDIS-02-19-0325-RE.

Duncan, R. W., Singh, S. P., and Gilbertson, R. L. (2011). Interaction of common bacterial blight bacteria with disease resistance quantitative trait Loci in common bean. *Phytopathology* 101, 425–435. doi:10.1094/PHYTO-03-10-0095.

Foucher, J., Ruh, M., Préveaux, A., Carrère, S., Pelletier, S., Briand, M., et al. (2020). Common bean resistance to Xanthomonas is associated with upregulation of the salicylic acid pathway and downregulation of photosynthesis. *BMC Genomics* 21, 1–18. doi:10.1186/s12864-020-06972-6.

Goodwin, P. H., and Sopher, C. R. (1994). Water stress in leaves of Phaseolus vulgaris infected with Xanthomonas campestris pv. phaseoli. *J. Phytopathol.* 140, 219–226.

Grimault, V., Olivier, V., Rolland, M., Darrasse, A., and Jacques, M.-A. A. (2014). "Detection of Xanthomonas axonopodis pv. phaseoli on Phaseolus vulgaris.," in *IST Association (ed) seed health methods: 7-021* (International Seed Testing Association (ISTA), Bassersdorf, Switzerland).

Hunt, M., Silva, N. De, Otto, T. D., Parkhill, J., Keane, J. A., and Harris, S. R. (2015). Circlator: Automated circularization of genome assemblies using long sequencing reads. *Genome Biol.* 16, 1–10. doi:10.1186/s13059-015-0849-0.

Ilett, M., Wills, J., Rees, P., Sharma, S., Micklethwaite, S., Brown, A., et al. (2020). Application of automated electron microscopy imaging and machine learning to characterise and quantify nanoparticle dispersion in aqueous media. *J. Microsc.* 279, 177–184. doi:10.1111/jmi.12853.

Koren, S., Walenz, B. P., Berlin, K., Miller, J. R., Bergman, N. H., and Phillippy, A. M. (2017). Canu: Scalable and accurate long-read assembly via adaptive κ-mer weighting and repeat

394 separation. *Genome Res.* 27, 722–736. doi:10.1101/gr.215087.116.
395 Mahlein, A.-K. (2016). Present and Future Trends in Plant Disease Detection. *Plant Dis.* 100, 1–
396 11. doi:10.1007/s13398-014-0173-7.2.
397 Méline, V., Brin, C., Lebreton, G., Ledroit, L., Sochard, D., Hunault, G., et al. (2020). A
398 Computation Method Based on the Combination of Chlorophyll Fluorescence Parameters to
399 Improve the Discrimination of Visually Similar Phenotypes Induced by Bacterial Virulence
400 Factors. *Front. Plant Sci.* 11, 1–14. doi:10.3389/fpls.2020.00213.
401 Mkandawire, A. B. C., Mabagala, R. B., Guzmán, P., Gepts, P., and Gilbertson, R. L. (2004).
402 Genetic Diversity and Pathogenic Variation of Common Blight Bacteria (Xanthomonas
403 campestris pv . phaseoli and X . campestris pv . phaseoli var . fuscans) Suggests Pathogen
404 Coevolution with the Common Bean. 94, 593–603.
405 Monteiro, A. L. R., Chaves, F. S., Pantaleão, A. S. L., Carneiro, P. C. S., de Souza Carneiro, J.
406 E., and Badel, J. L. (2020). Sources, spectrum, genetics, and inheritance of phaseolus
407 vulgaris resistance against xanthomonas citri pv. fuscans. *Phytopathology* 110, 1428–1436.
408 doi:10.1094/PHYTO-01-20-0020-R.
409 Nutter, F. W., Esker, P. D., and Netto, R. A. C. (2006). Disease assessment concepts and the
410 advancements made in improving the accuracy and precision of plant disease data. *Eur. J.*
411 *Plant Pathol.* 115, 95–103. doi:10.1007/s10658-005-1230-z.
412 Ojeda-Martinez, D., Martinez, M., Diaz, I., and Santamaria, M. E. (2020). Saving time
413 maintaining reliability: a new method for quantification of Tetranychus urticae damage in
414 Arabidopsis whole rosettes. *BMC Plant Biol.* 20, 397. doi:10.1186/s12870-020-02584-0.
415 Opio, A. ., Teri, J. ., and Allen, D. . (1993). Studies on Seed Transmission of Xanthomonas
416 campestris pv phaseoli in Common Beans in Uganda. *African Crop Sci. J.* 1, 59–67.
417 Pastor-Corrales, M. A., Beebe, S. E., and Corree, F. J. (1981). Comparing 2 Inoculation

418 Techniques for Evaluating Resistance in Beans to Xanthomonas campestrís. *Cent. Int. Agric.*
419 *Trop.*, 193–503.
420 Pike, J. A., Simms, V. A., Smith, C. W., Morgan, N. V., Khan, A. O., Poulter, N. S., et al. (2020).
421 An adaptable analysis workflow for characterization of platelet spreading and morphology.
422 *Platelets* 7104. doi:10.1080/09537104.2020.1748588.
423 Poland, J. A., and Nelson, R. J. (2010). In the eye of the beholder: The effect of rater variability
424 and different rating scales on QTL mapping. *Phytopathology* 101, 290–298.
425 doi:10.1094/PHYTO-03-10-0087.
426 Popovic, T., Starovic, M., Aleksic, G., Zivkovic, S., Josic, D., Ignjatov, M., et al. (2012).
427 Response of different beans against common bacterial blight disease caused by
428 Xanthomonas axonopodis PV. phaseoli. *Bulg. J. Agric. Sci.* 18, 701–707.
429 Pritchard, L., Glover, R. H., Humphris, S., Elphinstone, J. G., and Toth, I. K. (2016). Genomics
430 and taxonomy in diagnostics for food security: Soft-rotting enterobacterial plant pathogens.
431 *Anal. Methods* 8, 12–24. doi:10.1039/c5ay02550h.
432 Rashid, R., Gaglia, G., Chen, Y. A., Lin, J. R., Du, Z., Maliga, Z., et al. (2019). Highly
433 multiplexed immunofluorescence images and single-cell data of immune markers in tonsil
434 and lung cancer. *Sci. data* 6, 323. doi:10.1038/s41597-019-0332-y.
435 Rodríguez De Luque, J. J., and Creamer, B. (2014). Major constraints and trends for common
436 bean production and commercialization; establishing priorities for future research. *Agron.*
437 *Colomb.* 32, 423–431. doi:10.15446/agron.colomb.v32n3.46052.
438 Rousseau, C., Belin, E., Bove, E., Rousseau, D., Fabre, F., Berruyer, R., et al. (2013). High
439 throughput quantitative phenotyping of plant resistance using chlorophyll fluorescence
440 image analysis. *Plant Methods* 9, 1–13. doi:10.1186/1746-4811-9-17.
441 Rousseau, C., Hunault, G., Gaillard, S., Bourbeillon, J., Montiel, G., Simier, P., et al. (2015).

Phenoplant: A web resource for the exploration of large chlorophyll fluorescence image datasets. *Plant Methods* 11, 24. doi:10.1186/s13007-015-0068-4.

Ruh, M., Briand, M., Bonneau, S., Jacques, M.-A., and Chen, N. W. G. (2017). Xanthomonas adaptation to common bean is associated with horizontal transfers of genes encoding TAL effectors. *BMC Genomics* 18, 670. doi:10.1186/s12864-017-4087-6.

Schäfer, A., Tauch, A., Jsger, W., Kalinowski, J., Thierbachb, G., and Piihler, A. (1994). Small mobilizable multi-purpose cloning vectors derived from the Escherichia coli plasmids pK18 and pK19: selection of defined deletions in the chromosome of Corynebacterium glutumicum. *Gene* 145, 49–5201.

Schindelin, J., Arganda-Carreras, I., Frise, E., Kaynig, V., Longair, M., Pietzsch, T., et al. (2012). Fiji: An open-source platform for biological-image analysis. *Nat. Methods* 9, 676–682. doi:10.1038/nmeth.2019.

Seemann, T. (2014). Prokka: Rapid prokaryotic genome annotation. *Bioinformatics* 30, 2068–2069. doi:10.1093/bioinformatics/btu153.

Singh, S. P., and Miklas, P. N. (2015). Breeding Common Bean for Resistance to Common Blight : A Review. doi:10.2135/cropsci2014.07.0502.

Streubel, J., Blücher, C., Landgraf, A., and Boch, J. (2012). TAL effector RVD specificities and efficiencies. *Nat. Biotechnol.* 30, 593–595. doi:10.1038/nbt.2304.

Tugume, J. K., Tusiime, G., Sekamate, A. M., Buruchara, R., and Mukankusi, C. M. (2018). Diversity and interaction of common bacterial blight disease-causing bacteria (Xanthomonas spp.) with Phaseolus vulgaris L. *Crop J.* 7, 1–7. doi:10.1016/j.cj.2018.10.002.

Vidaver, A. K. (1993). *Xanthomonas campestris pv. phaseoli: cause of common bacterial blight of bean*. J. G. Swin. , ed. U. C. & H. London.

Xie, W., Yu, K., Pauls, K. P., and Navabi, A. (2012). Application of image analysis in studies of

quantitative disease resistance, exemplified using common bacterial blight-common bean pathosystem. *Phytopathology* 102, 434–442. doi:10.1094/PHYTO-06-11-0175.

Yu, K., Shi, C., and Zhang, B. (2012). Development and Application of Molecular Markers to Breed Common Bean (Phaseolus vulgaris L .) for Resistance to Common Bacterial Blight (CBB). *Appl. Photosynth.*, 365–388.

Zapata, M. (2006). A proposal for a uniform screening procedure for the reennhouse evalualtion of variability of Xanthomonas axonopodis pv. phaseoli and resistance on leaves of Phaseolus vulgaris. *Annu. Rep. Bean Improv. Coop.*, 213–214.

Zaumeyer, W. J., and Thomas, H. R. (1957). A monographic study of bean diseases and methods for their control. *Tech. Bull. 169625, United States Dep. Agric. Econ. Res. Serv.*

SUPPORTING INFORMATION LEGENDS

Table S1. List of primers used for *tal* mutagenesis

Supplemental Figure 1: Comparison between MLI and CFI after rub-inoculation of first leaves. First leaves of bean plants were inoculated by rubbing with strain CFBP6165R. Images were taken 14 days after inoculation. Each line shows the two first leaves of a same plant. Pixels corresponding to estimated symptoms are in red. MLI: machine learning-based imagery; CFI: chlorophyll fluorescence imagery.

Supplemental Figure 2: Comparison between MLI and CFI after dip-inoculation of trifoliate leaves. First trifoliate leaves were inoculated with strains CFBP6165R, 6165RD*tal22B*, CFBP6546R, 6546RD*tal18H* or distilled water as control. Images were taken 12 days after inoculation. For each condition, 15 leaflets coming from five different plants were analysed. (**a)** Symptomatic areas measured using chlorophyll fluorescence imagery (CFI) or machine learning-based imagery (MLI). **(b)** Images corresponding to the leaflets with symptoms closest to the mean

disease area as estimated by MLI in **(a)**. Pixels corresponding to estimated symptoms are in red.

FIGURE LEGENDS

Figure 1. Strain 6546R is more aggressive than strain 6165R. Images were taken at 14 days post inoculation, and evaluation of symptoms was done by chlorophyll fluorescence imaging on trifoliate leaves inoculated by dipping (**a, b, c**), or by machine learning-based imaging on first leaves inoculated by rubbing (**d, e, f**). Experiments were repeated twice independently, with five plants per assay, and concatenated (n=10 plants). Box-plots represent the percentage of symptomatic area per plant and *p*-values were calculated by Mann-Whitney test. The images correspond to leaves or leaflets presenting the closest symptom percentages to the median values. The symptoms detected appear in red on the surface of the leaf in white. White bars correspond to 1 centimeter.

Figure 2. Description of *tal* mutant strains 6546RΔ*tal18H* (**a**, **c**, **e**) and 6165RΔ*tal22B* (**b**, **d**, **f**). Western blot analysis of TALEs (**a**, **b**). Graphical map of plasmids from *tal* mutant strains using GView (Petkau et al., 2010) with corresponding wild-type strains as references (**c**, **d**). The deletion observed in plasmid C from 6546RΔ*tal18H* corresponds to *tal18H* while the deletion in plasmid A from 6165RΔ*tal22B* corresponds to *tal22B* (**d**). Bacterial growth dynamics of wild-type and mutant strains (**e**, **f**). Growth assays were done as biological duplicates with technical triplicates. Bars represent standard deviation.

Figure 3. Pathogenicity of 6546RΔ*tal18H* compared to wild-type strain 6546R. Images were taken at 14 days post inoculation. Evaluation of symptoms was done by chlorophyll fluorescence imaging on trifoliate leaves inoculated by dipping (**a**, **b**, **c**), or by machine learning-based imaging on first leaves inoculated by rubbing (**d**, **e**, **f**). Experiments were repeated twice independently, with eight plants per assay, and concatenated (n=16 plants). Box-plots represent the percentage of

symptomatic area per plant and *p*-values were calculated by Mann-Whitney test. The images correspond to leaves or leaflets presenting the closest symptom percentages to the median values. The symptoms detected appear in red on the surface of the leaf in white. White bars correspond to 1 centimeter.

Figure 4. Pathogenicity of 6165RΔ*tal22B* compared to wild-type strain 6165R. Images were taken at 14 days post inoculation. Evaluation of symptoms was done by chlorophyll fluorescence imaging on trifoliate leaves inoculated by dipping (**a**, **b**, **c**), or by machine learning-based imaging on first leaves inoculated by rubbing (**d**, **e**, **f**). Experiments were repeated twice independently, with five plants per assay, and concatenated (n=10 plants). Box-plots represent the percentage of symptomatic area per plant and *p*-values were calculated by Mann-Whitney test. The images correspond to leaves or leaflets presenting the closest symptom percentages to the median values. The symptoms detected appear in red on the surface of the leaf in white. White bars correspond to 1 centimeter.

Figure 5. Correlation between different symptom quantification methods. Trifoliate leaves were inoculated by dipping with either H2O or strains 6165R, 6165RΔ*tal22B*, 6546R and 6546RΔ*tal18H*. For each leaflet, both chlorophyll fluorescence and RGB images were taken at 14 days post inoculation. Expert visual assessment of symptom percentage was performed on RGB images using the scale by Opio et al. (1993) and results were compared to chlorophyll fluorescence imaging (CFI, **a**) or machine learning-based imaging (MLI, **b**). The regression line formula and correlation coefficient (R^2) were calculated with Excel, using 15 leaflets per condition (75 in total).

Table 1. Characteristics of pathogenicity tests.

	Trifoliate dipping + CFI[a]	**First leaf rubbing + MLI[b]**
Discriminating power	Poor	Good
Detection of non-visible symptoms	Yes	No
Plant growing time	15 days	8 days
Symptom assessment date	14 days post inoculation	14 days post inoculation
Duration of a trial	29 days	22 days
Plants with homogeneous leaves	84%	93%
Average time of inoculation per plant	150 seconds	43 seconds
Volume per inoculum	500 mL	25 mL
Equipment	PSI Open FluorCam FC 800-O or equivalent	Light table and camera
Average image taking time per plant	327 seconds	45 seconds
Image analysis software	Phenoplant	Ilastik

[a]CFI: chlorophyll fluorescence imaging
[b]MLI: machine learning-based imaging

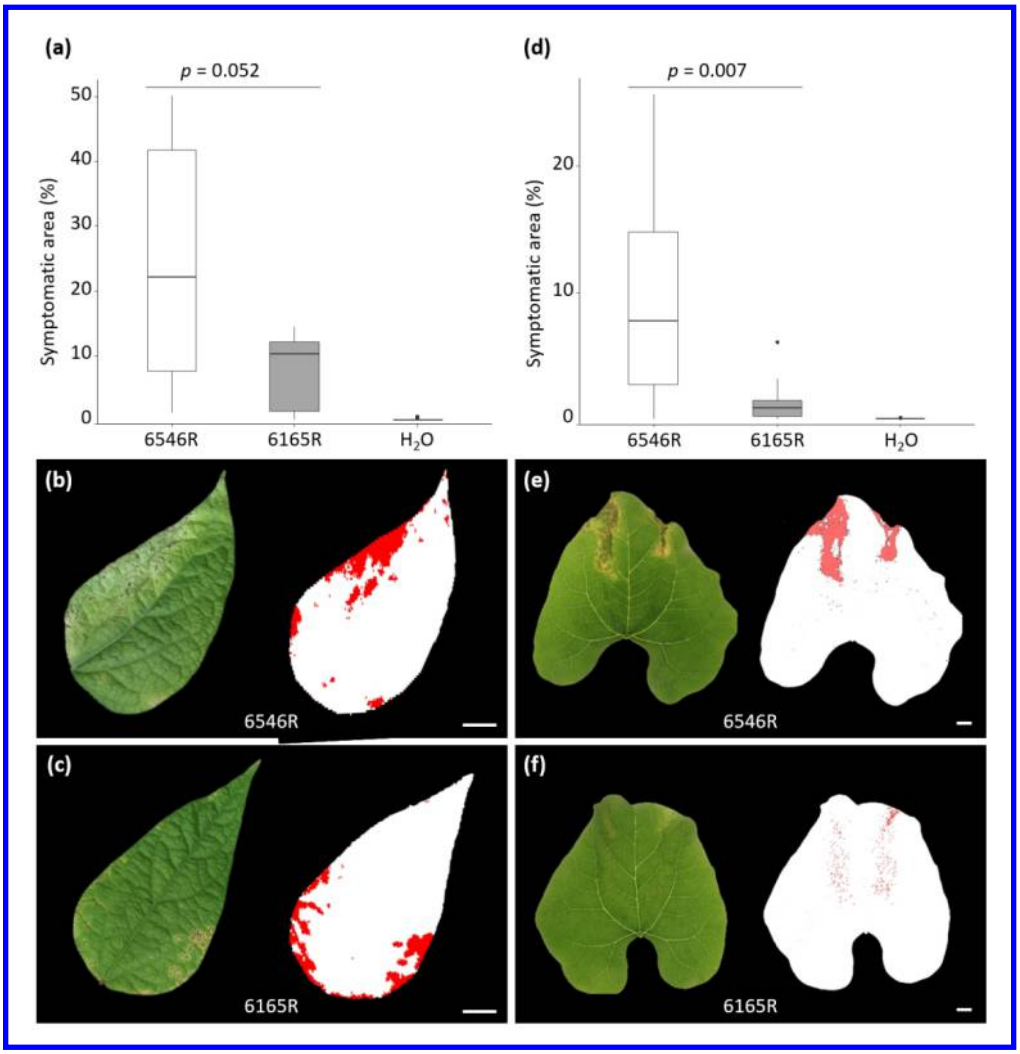

Figure 1. Strain 6546R is more aggressive than strain 6165R. Images were taken at 14 days post inoculation, and Evaluation of symptoms was done by chlorophyll fluorescence imaging on trifoliate leaves inoculated by dipping (a, b, c), or by machine learning-based imaging on first leaves inoculated by rubbing (d, e, f). Experiments were repeated twice independently, with five plants per assay, and concatenated (n=10 plants). Box-plots represent the percentage of symptomatic area per plant and p-values were calculated by Mann-Whitney test. The images correspond to leaves or leaflets presenting the closest symptom percentages to the median values. The symptoms detected appear in red on the surface of the leaf in white. White bars correspond to 1 centimeter.

266x274mm (150 x 150 DPI)

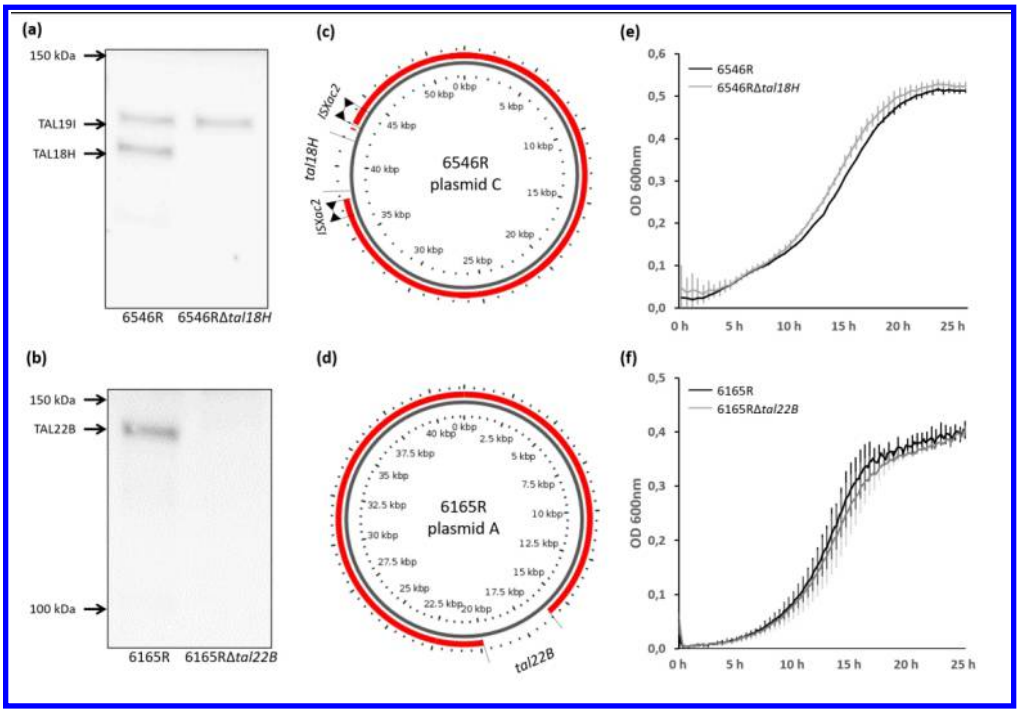

Figure 2. Description of tal mutant strains 6546RΔtal18H (a, c, e) and 6165RΔtal22B (b, d, f). Western blot analysis of TALEs (a, b). Graphical map of plasmids from tal mutant strains using GView (Petkau et al., 2010) with corresponding wild-type strains as references (c, d). The deletion observed in plasmid C from 6546RΔtal18H corresponds to tal18H while the deletion in plasmid A from 6165RΔtal22B corresponds to tal22B (d). Bacterial growth dynamics of wild-type and mutant strains (e, f). Growth assays were done as biological duplicates with technical triplicates. Bars represent standard deviation.

351x242mm (150 x 150 DPI)

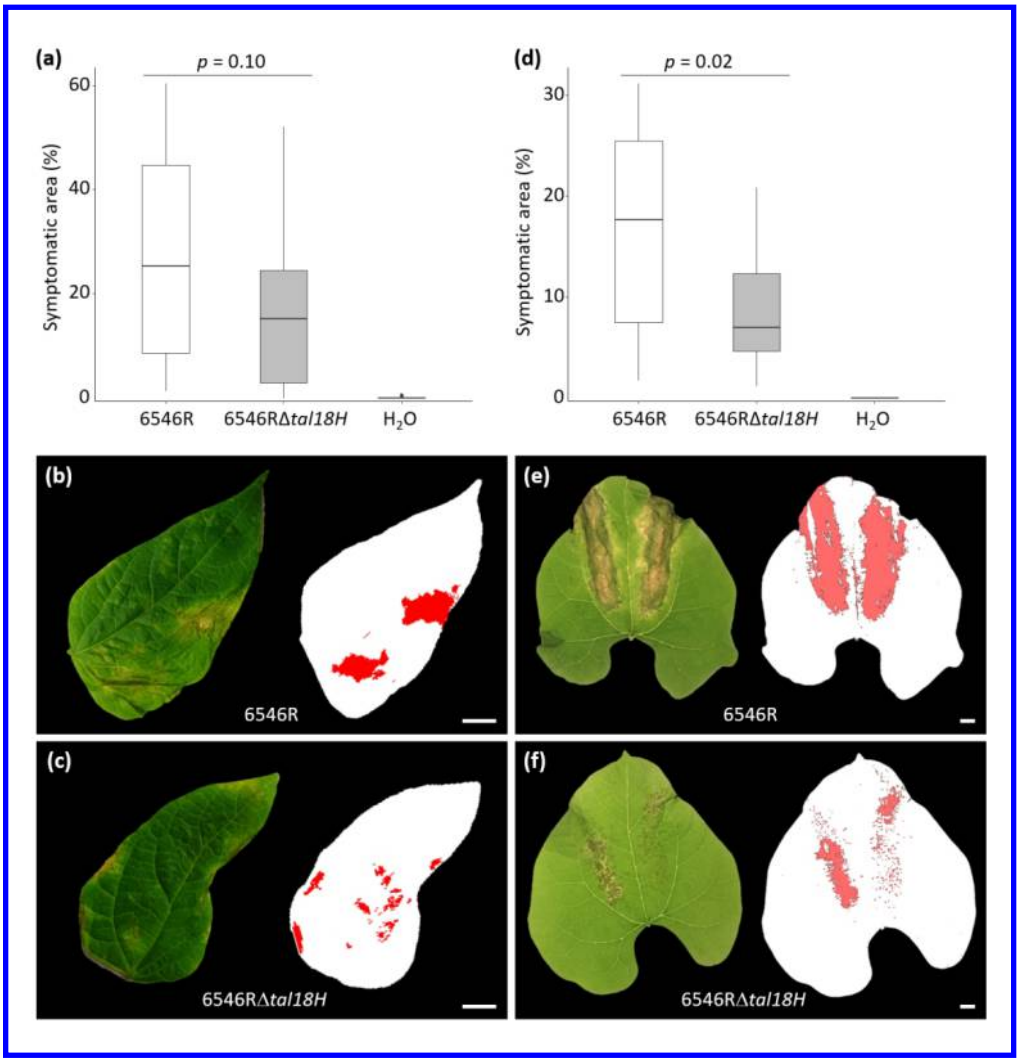

Figure 3. Pathogenicity of 6546RΔtal18H compared to wild-type strain 6546R. Images were taken at 14 days post inoculation. Evaluation of symptoms was done by chlorophyll fluorescence imaging on trifoliate leaves inoculated by dipping (a, b, c), or by machine learning-based imaging on first leaves inoculated by rubbing (d, e, f). Experiments were repeated twice independently, with eight plants per assay, and concatenated (n=16 plants). Box-plots represent the percentage of symptomatic area per plant and p-values were calculated by Mann-Whitney test. The images correspond to leaves or leaflets presenting the closest symptom percentages to the median values. The symptoms detected appear in red on the surface of the leaf in white. White bars correspond to 1 centimeter.

266x277mm (150 x 150 DPI)

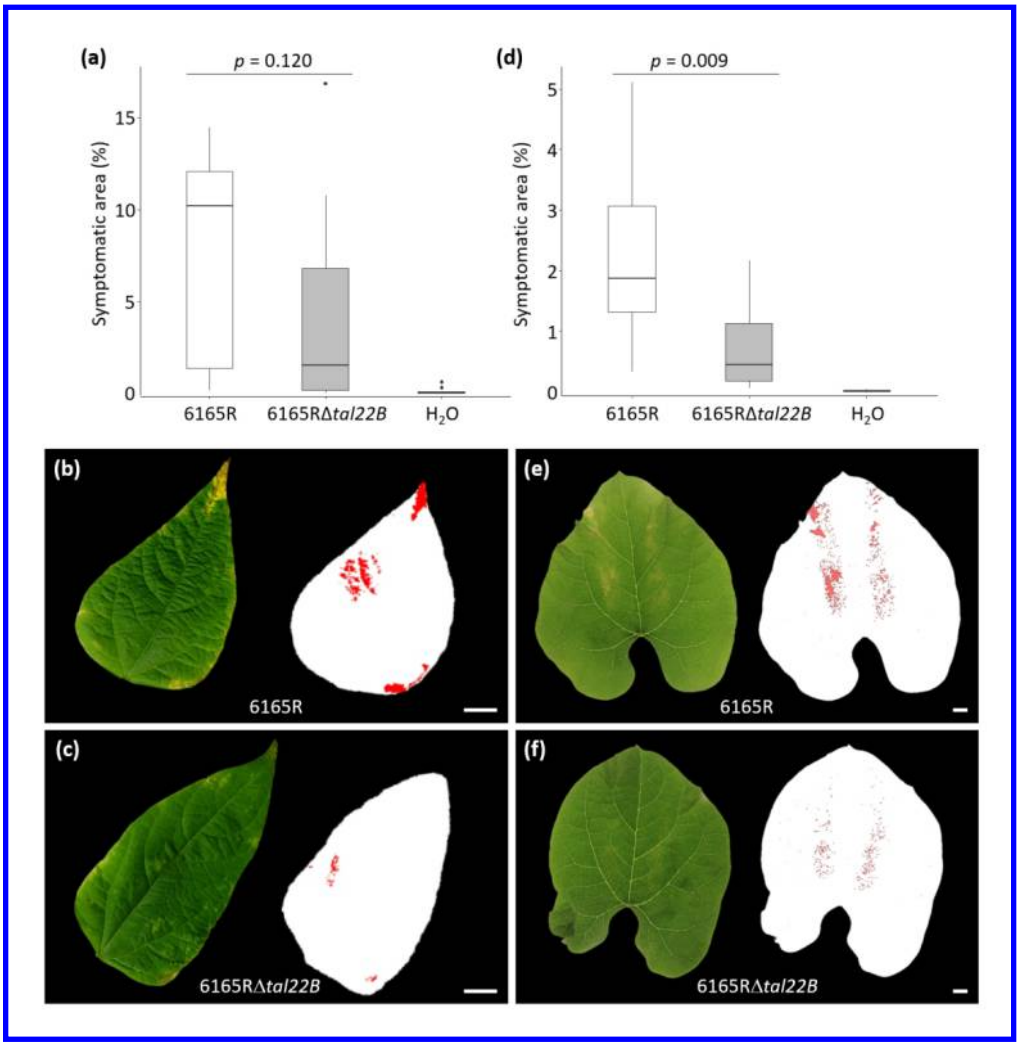

Figure 4. Pathogenicity of 6165RΔtal22B compared to wild-type strain 6165R. Images were taken at 14 days post inoculation. Evaluation of symptoms was done by chlorophyll fluorescence imaging on trifoliate leaves inoculated by dipping (a, b, c), or by machine learning-based imaging on first leaves inoculated by rubbing (d, e, f). Experiments were repeated twice independently, with five plants per assay, and concatenated (n=10 plants). Box-plots represent the percentage of symptomatic area per plant and p-values were calculated by Mann-Whitney test. The images correspond to leaves or leaflets presenting the closest symptom percentages to the median values. The symptoms detected appear in red on the surface of the leaf in white. White bars correspond to 1 centimeter.

271x277mm (150 x 150 DPI)

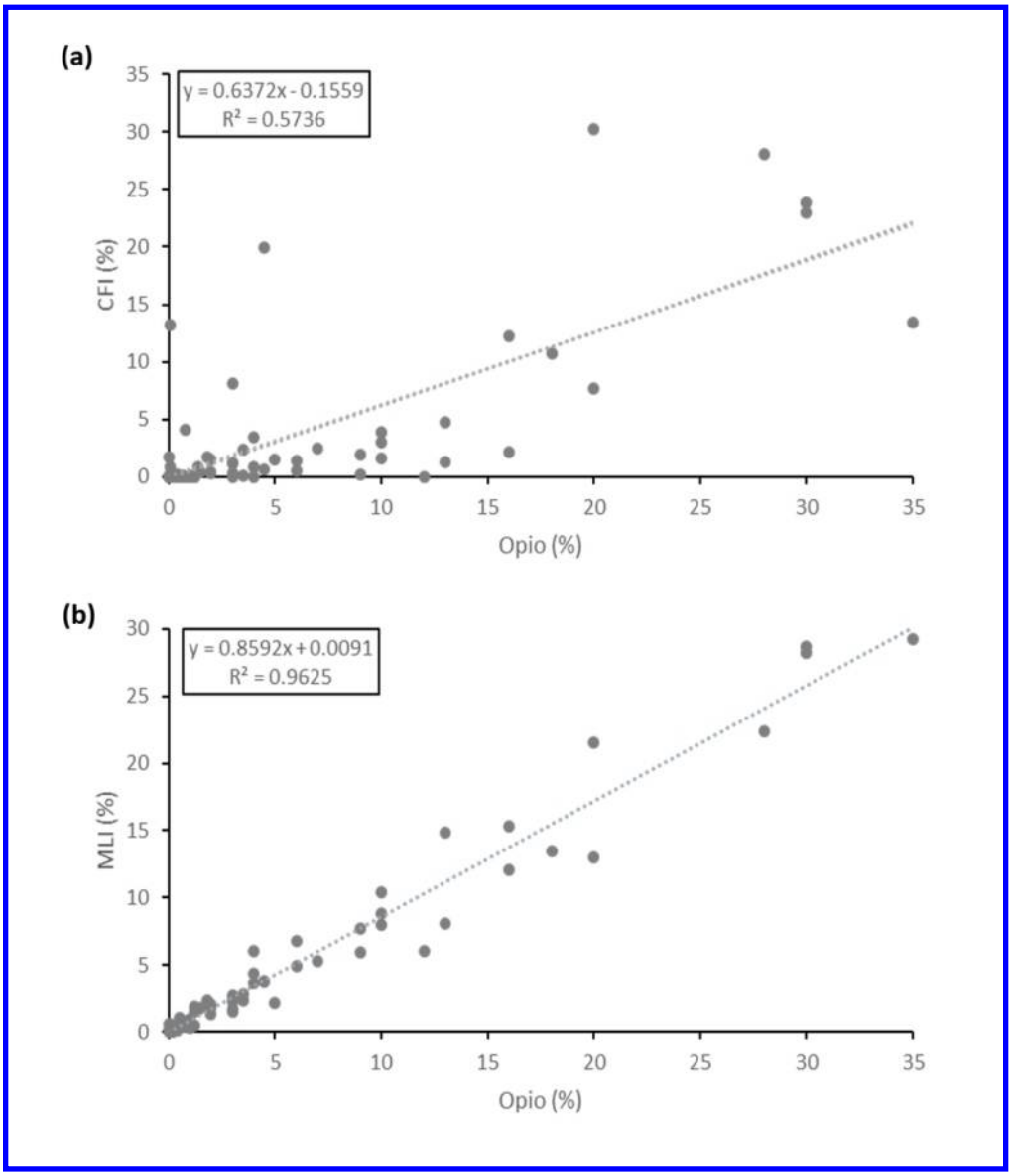

Figure 5. Correlation between different symptom quantification methods. Trifoliate leaves were inoculated by dipping with either H2O or strains 6165R, 6165RΔtal22B, 6546R and 6546RΔtal18H. For each leaflet, both chlorophyll fluorescence and RGB images were taken at 14 days post inoculation. Expert visual assessment of symptom percentage was performed on RGB images using the scale by Opio et al. (1993) and results were compared to chlorophyll fluorescence imaging (CFI, a) or machine learning-based imaging (MLI, b). The regression line formula and correlation coefficient (R2) were calculated with Excel, using 15 leaflets per condition (75 in total).

240x278mm (150 x 150 DPI)

Supplemental Figure 2: Comparison between MLI and CFI after dip-inoculation of first trifoliate leaves. First trifoliate leaves were inoculated with strains CFBP6165R, 6165RΔ*tal22B*, CFBP6546R, 6546RΔ*tal18H* or distilled water as control. Images were taken 12 days after inoculation. For each condition, 15 leaflets coming from five different plants were analysed. (**a)** Symptomatic areas measured using chlorophyll fluorescence imagery (CFI) or machine learning-based imagery (MLI). **(b)** Images corresponding to the leaflets with symptoms closest to the mean disease area as estimated by MLI in **(a)**. Pixels corresponding to estimated symptoms are in red.

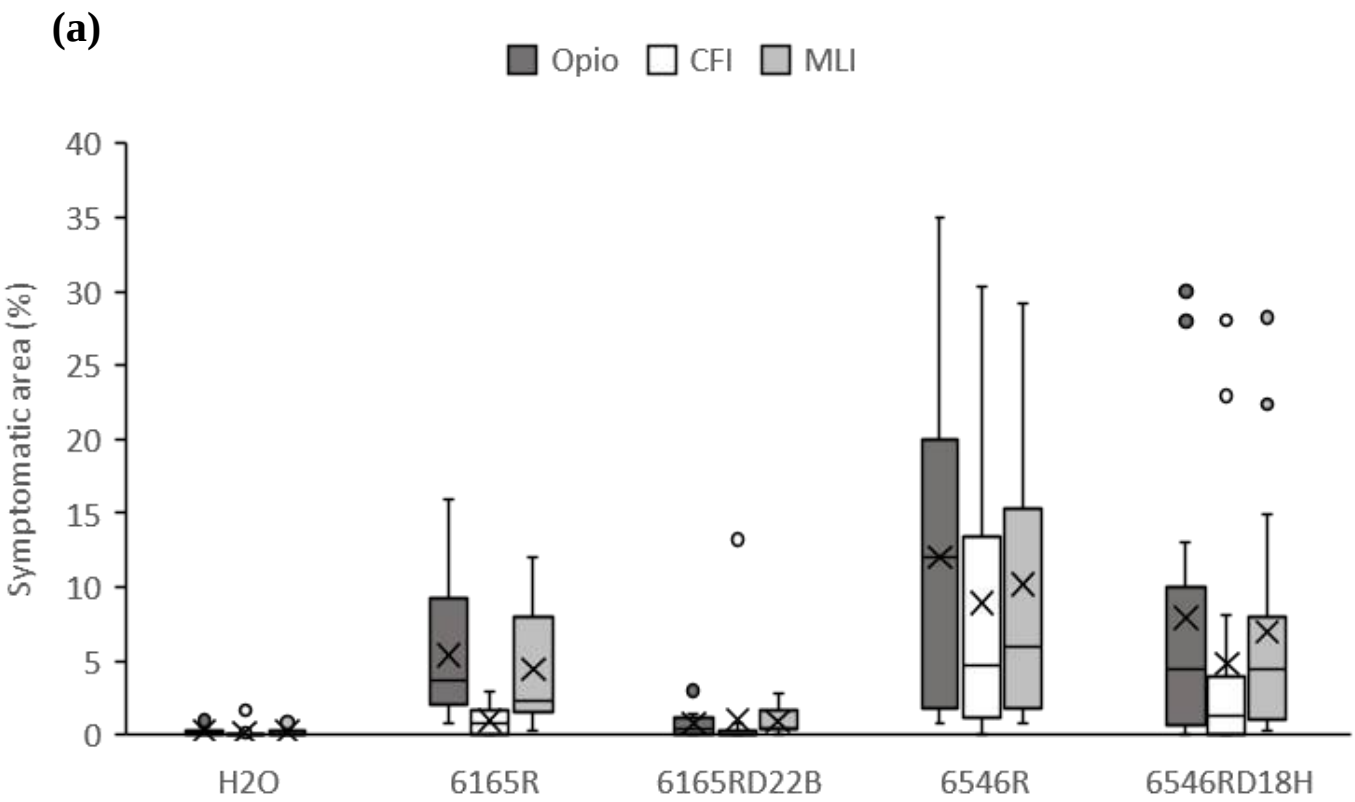

(b)

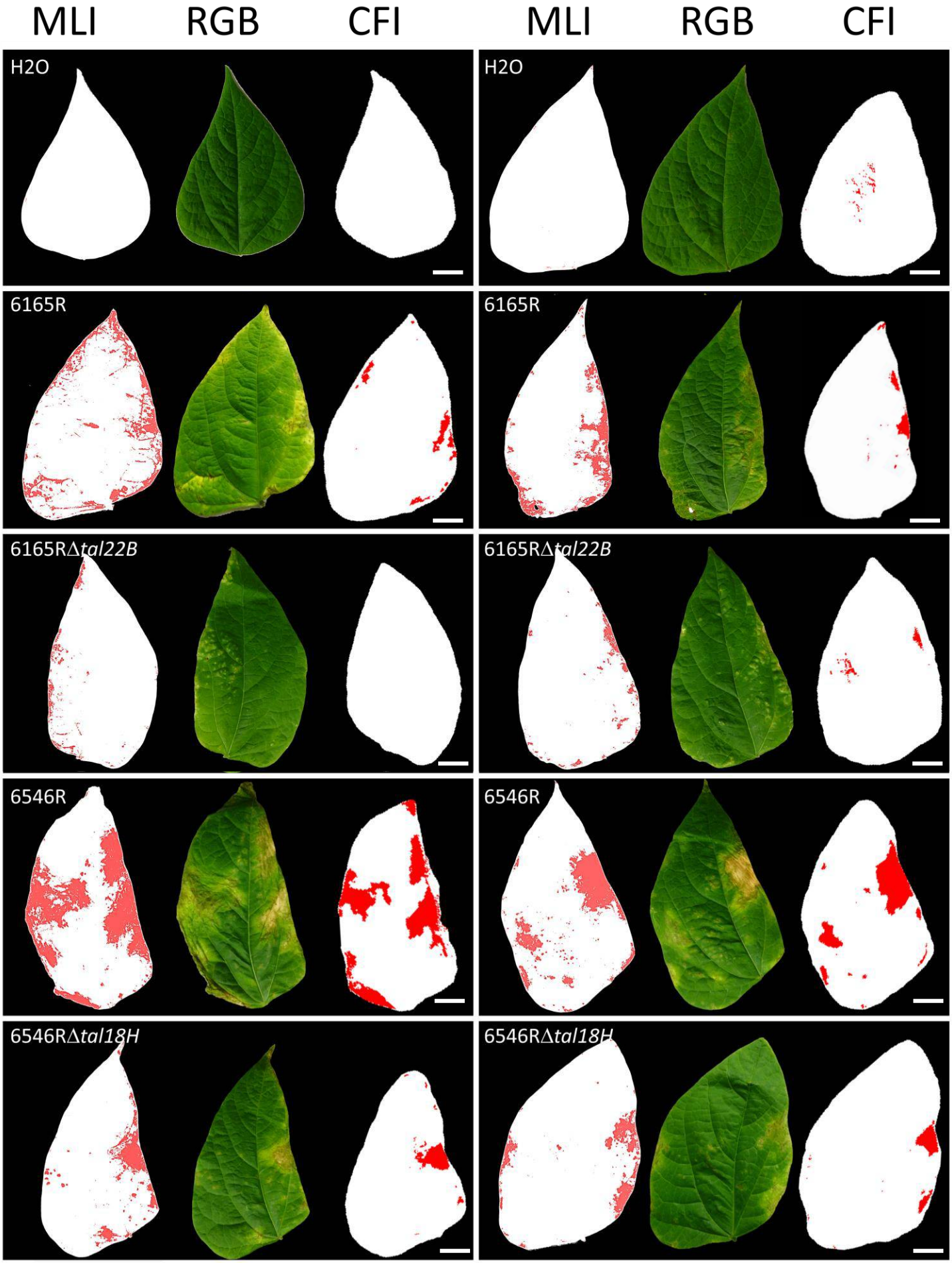
MLI
RGB
CFI
MLI
RGB
CFI
H2O
H2O
6165R
6165R
6165RΔtal22B
6165RΔtal22B
6546R
6546R
6546RΔtal18H
6546RΔtal18H